JACS
JOURNAL OF THE AMERICAN CHEMICAL SOCIETY
pubs.acs.org/JACS
Article

Photocatalytic Extraction of Uranium from Seawater Using Covalent Organic Framework Nanowires

Xujiao Ma, Katie R. Meihaus, Yajie Yang, Yue Zheng, Fengchao Cui, Jixiang Li, Yanqin Zhao, Biao Jiang, Ye Yuan,* Jeffrey R. Long,* and Guangshan Zhu*

Cite This: J. Am. Chem. Soc. 2024, 146, 23566−23573

Read Online

ACCESS | Metrics & More | Article Recommendations | Supporting Information

ABSTRACT: In the push to achieve net-zero emissions by 2050, nuclear power will play an essential role alongside renewable wind and solar power, and correspondingly global interest and investment in this well-established technology is accelerating. The uranium present in seawater could support nuclear power generation for centuries, but traditional adsorptive separation strategies have proven ineffective for the selective extraction of uranium from this vast resource. Here, we report the synthesis of nanowires of a triazine-linked two-dimensional covalent organic framework via a solvent modulation approach, which can be used to access nanowire external diameters ranging from 50 to 200 nm. The 100 nm nanowires are exceptionally promising for the capture of uranium(VI) via photocatalytic reduction. Under simulated sunlight and without the use of sacrificial agents, the nanowires achieve a uranium uptake of 10.9 g/g from a 100 ppm uranyl(VI) solution, which is the highest reported to date among materials studied for photo and electrocatalytic uranium capture. Significantly, these nanowires exhibit a uranium adsorption capacity of 34.5 mg/g after exposure to seawater under irradiation for 42 days, a record among all materials reported to date for uranium capture.

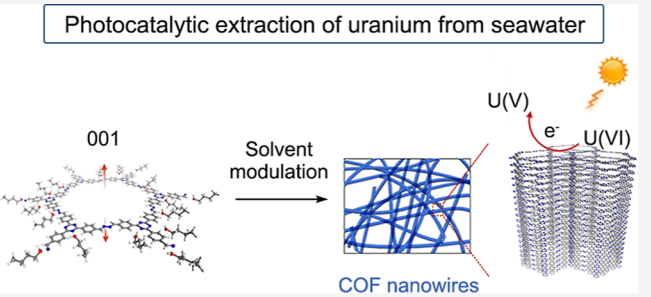

INTRODUCTION

Energy shortages and the increasingly harmful effects of climate change are driving the expansion of clean energy resources.[1−6] Nuclear power is the only mature technology that can continuously provide electricity on a large scale with ultralow greenhouse gas emission.[7,8] Over the next two decades, nuclear power is projected to be the second fastest-growing global energy source after renewables[9] and will play a critical role in achieving net-zero emissions by 2050.[2] Seawater is a vast untapped source of uranium that could support nuclear power production for centuries.[10,11] As such, the extraction of uranium from seawater has been identified as one of seven critical separations for global prosperity.[3] Decades of research focused on the development of materials for adsorptive uranium separations has met with limited success,[6,11−13] because uranium is present in seawater at very low concentrations (∼3 ppb) together with numerous other ions that compete for binding or impede uranium diffusion and access to binding sites. Even state-of-the-art amidoxime-functionalized polymers have limited practical utility as a result of their poor selectivity for uranium over vanadium.[14]

An alternative strategy for the low-energy, selective recovery of uranium from seawater is sunlight-driven photocatalytic reduction of uranium(VI).[15] Traditional semiconductors such as TiO_2 and graphitic carbon nitride and porous solids such as metal−organic frameworks[16] and π-conjugated two-dimensional covalent organic frameworks (COFs) have been developed for this purpose,[7,17] but significant improvements are needed to enhance photocatalyst performance in the absence of sacrificial agents, under sunlight, and in real seawater. Given their unique optoelectronic properties and robust, tunable structures, semiconducting COFs are a promising platform for the development of photocatalysts for uranium recovery, and they have attracted significant interest for applications in photocatalysis more broadly.[18−20] In parallel, there is growing interest in the use of low-dimensional semiconductor morphologies, such as nanocrystals and nanowires, for applications in photocatalysis, given their unique charge transport properties and high surface-area-to-volume ratios, which can contribute to significantly enhanced performance over that of their bulk counterparts.[21]

Herein, we describe a solvent modulation approach that affords access to nanowires of a triazine-linked two-dimensional (2D) COF with external diameters ranging from 50 to 200 nm, a morphology that, to our knowledge, has not

Received: June 7, 2024
Revised: July 28, 2024
Accepted: July 29, 2024
Published: August 9, 2024

https://doi.org/10.1021/jacs.4c07699
J. Am. Chem. Soc. 2024, 146, 23566−23573

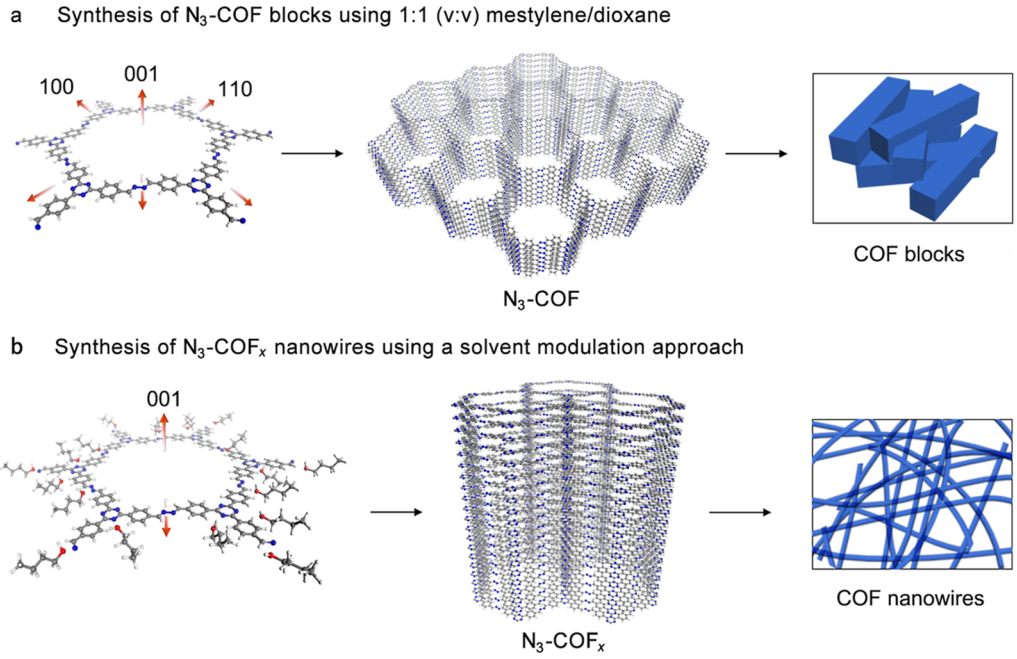

Figure 1. (a) Synthesis of the triazine-linked two-dimensional N_3-COF (*P6/m* space group) using a 1:1 mixture of mesitylene and dioxane yields COF nanocrystals with block morphology.[22] (b) Preferential growth of N_3-COF along the 001 direction is favored with the addition of *n*-butanol solvent, enabling the synthesis of N_3-COF$_x$ nanowires of varying diameters.

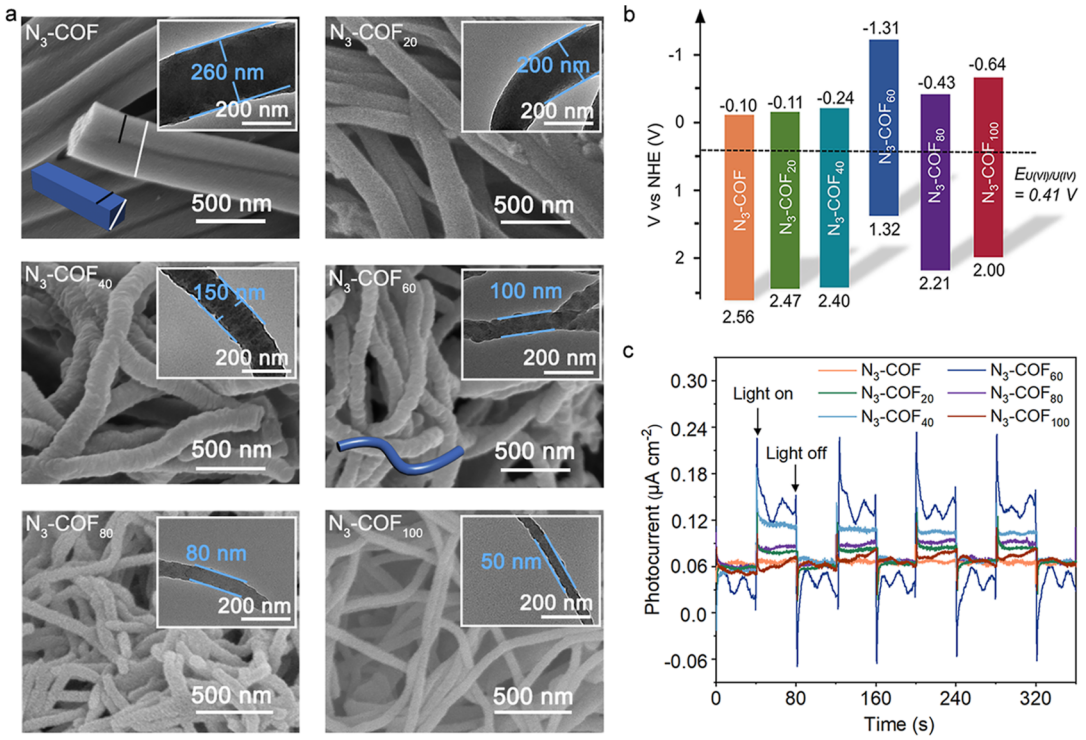

Figure 2. (a) SEM and TEM (inset) images of N_3-COF and N_3-COF$_x$ (x = 20, 40, 60, 80, 100). The blue lines are guides for the eye to indicate the width of the COF nanowires. SEM scale bar: 500 nm; TEM scale bar: 200 nm. (b) Band energy diagrams of N_3-COF and N_3-COF$_x$. (c) Transient photocurrent response of N_3-COF and N_3-COF$_x$.

previously been demonstrated for COFs (Figure 1a). Through a detailed investigation of the optoelectronic properties of these nanowires, we find that the 100 nm nanowires are promising photocatalysts for the capture of uranium from aqueous solutions. Under simulated sunlight and without the use of sacrificial agents, the nanowires capture 10.9 g U/g from a 100 ppm uranyl(VI) solution, which is the highest capacity reported to date for photo- or electrocatalytic uranium capture. Structural and spectroscopic analyses suggest that uranium uptake occurs via a mechanism involving initial reduction to U(V) followed by disproportionation. Finally, the nanowires exhibit a uranium adsorption capacity of 34.5 mg/g after exposure to commercial seawater for 42 days, a record among all materials reported to date that also exceeds the one-pass

https://doi.org/10.1021/jacs.4c07699
J. Am. Chem. Soc. 2024, 146, 23566−23573

capacity required for a material to be competitive with land-based uranium recovery.[11]

RESULTS AND DISCUSSION

The material N_3-COF was chosen for this study based on its excellent water stability and demonstrated performance as a visible-light photocatalyst for generating hydrogen from water.[22] When prepared using a 1:1 mixture of mesitylene and dioxane, N_3-COF forms as nanocrystallites with a rod-like morphology (Figure 1a),[22] which suggested to us the possibility of using a solvent-mediated strategy to promote growth along the long axis of the rod [the (001) direction] to form crystalline nanowires.[23] Of note, most COFs known to date form as irregular bulk powders or particles, morphologies that limit their visible light absorption and contribute to photoelectron−hole recombination.[24,25] However, advances in COF synthesis have enabled the isolation of micrometer-sized single crystals[26] and crystallites with varying morphologies, such as rods,[22] hollow tubes, nanofibers,[27] and spheres.[24]

We carried out molecular dynamic simulations using Gaussian 16 to determine the interaction energy between an N_3-COF fragment and dioxane, mesitylene, or *n*-butanol. The results indicated that the fragments interact most strongly with *n*-butanol, followed by mesitylene and dioxane (see the Materials and Methods for details and Figure S1). In particular, *n*-butanol was predicted to concentrate at the 100 and 110-crystal planes via stabilizing hydrogen-bonding interactions and might thereby be expected to inhibit growth in the *ab* plane and promote the formation of N_3-COF along the 001-crystal direction, leading to oriented nanowires.

A series of crystalline N_3-COF samples were synthesized using 1:1 (v/v) mesitylene and dioxane (no *n*-butanol), a mixture of 1:1 mesitylene and dioxane with a balance of *n*-butanol (20, 40, 60, or 80%), or 100% *n*-butanol, hereafter referred to as N_3-COF and N_3-COF$_x$ (x = 20, 40, 60, 80, 100), respectively. Fourier transform infrared spectra collected for all samples confirmed the successful coupling of hydrazine and 2,4,6-tris(4-formylphenyl)-1,3,5-triazine to form the network solids (Figure S2). In addition to the absence of an N−H stretch from hydrazine (3500 cm^{-1}), the spectra feature a C═N stretch at 1619 cm^{-1}. Raman spectra obtained for all samples feature an N−N stretch at 985 cm^{-1} and an asymmetric C═N stretch between 1600 and 1625 cm^{-1} (Figure S3). Analysis of the samples using scanning electron microscopy (SEM) and transmission electron microscopy (TEM) revealed the formation of rod-like crystallites in the case of N_3-COF and one-dimensional nanostructures in the case of N_3-COF$_x$, with diameters decreasing from 200 to 50 nm with increasing x (Figure 2a). Powder X-ray diffraction (PXRD) analysis of N_3-COF revealed a strong (100) reflection at 2θ = 3.52° and a series of peaks at 6.0, 7.1, 9.5 and 26.4° corresponding to the (110), (200), (120), and (001) planes, respectively (Figure S4), consistent with the space group *P6/m* reported previously for this material.[22] For the N_3-COF$_x$ materials, the diffraction peak at 3.52° gradually broadened and diminished in intensity with increasing x, while the intensity of the peak at 26.4° increased, indicating the hindered growth along the 001 direction (Figure S4).

Nitrogen adsorption data collected at 77 K confirmed that N_3-COF and N_3-COF$_x$ are permanently porous, with Brunauer−Emmett−Teller (BET) surface areas of 1640 and 1200, 1120, 852, 910, and 1080 m^2/g for x = 20, 40, 60, 80, 100, respectively (Figures S5 and S6). The surface area for N_3-COF compares well with the previously reported value for this material (1537 m^2/g),[22] while the gradual decrease in surface area across the nanowire series up to N_3-COF$_{60}$ is attributed to the inhibition of the network growth in the 2D plane and a decrease in the corresponding internal surface area. The surface area increases for N_3-COF$_x$ (x = 80, 100), which we attribute to the further narrowing of the nanowire external diameters and an increase in the external surface area. Pore-size distributions were calculated for N_3-COF$_x$ using nonlocal density functional theory and found to be centered at approximately 26 Å (Figure S7), consistent with the pore size of 24 Å determined previously for N_3-COF.[22] The nanowires are highly robust, and after soaking in water for 14 days, there was no detectable change in their infrared spectra or PXRD patterns (Figures S8 and S9). Additionally, thermogravimetric analysis (TGA) revealed that the N_3-COF$_x$ materials are stable up to 450 °C in the air (Figure S10). This excellent thermal and water stability is ascribed to strong $\pi-\pi$ interactions between the 2D layers and suggests that the nanowires may be viable candidates for use in extracting uranium from seawater.

The UV−vis diffuse reflectance spectra of each COF sample are shown in Figure S11. The onset of light absorption for N_3-COF$_x$ is red-shifted by approximately 20 nm compared to the absorption of N_3-COF (384 nm), as expected due to the quantum size effect.[28] Using the Kubelka−Munk function, the optical band gap for N_3-COF was determined to be 2.66 eV, while the optical band gaps for N_3-COF$_x$ are similar and range from 2.58 to 2.64 eV (Figure S11). The positive slope of Mott−Schottky plots for the COF nanowires indicates that they are n-type semiconductors in which most of the carriers are electrons (Figure S12). From the analysis of ultraviolet photoelectron spectra collected for N_3-COF and N_3-COF$_x$ (Figure S13; see Materials and Methods for details), the valence band maxima were found to range from 1.32 eV (for N_3-COF$_{60}$) to 2.56 eV (for N_3-COF) versus the normal hydrogen electrode (NHE). Together with the optical band gaps determined from UV−vis diffuse reflectance spectroscopy, these results were used to generate band energy diagrams for each material, as shown in Figure 2b. The conduction band maxima range from −1.31 eV for N_3-COF$_{60}$ to −0.10 eV for N_3-COF, and as such the nanowires theoretically provide enough driving force for the reduction of U^{VI} to U^{IV} ($E_{1/2}$ = 0.411 eV versus NHE[17]). For each material, the work function, φ, was calculated by subtracting E_{cutoff} (Figure S13a) from the photon energy of the He light source (21.22 eV) and found to be smallest for N_3-COF$_{60}$ and N_3-COF$_{80}$ (~3.3 eV), indicating that the electrons in these materials can more readily participate in photocatalysis[29] (Figure 2b).

The photoluminescence spectra for all N_3-COF samples feature a peak centered at 590 nm (Figure S14). In general, the fluorescence emission intensity of the nanowires was greater than that of N_3-COF, and N_3-COF$_{60}$ exhibited the highest fluorescence intensity (approximately an order of magnitude higher than that of N_3-COF).[30] Further, the Hall effect measurements were studied to quantify the carrier concentration. We concluded that N_3-COF and N_3-COF$_x$.were the n-type semiconductors, and N_3-COF$_{60}$ had the highest carrier concentration (1.96×10^{11} cm^3) (Table S1). Consistent with this result, N_3-COF$_{60}$ nanowires exhibited the strongest photocurrent intensity in transient photocurrent response measurements over the course of four cycles (Figure 2c).

https://doi.org/10.1021/jacs.4c07699
J. Am. Chem. Soc. 2024, 146, 23566−23573

Time-resolved photoluminescence attenuation spectroscopy was used to determine the average lifetime of the N_3-COF_x photocatalysts. The fluorescence lifetime of N_3-COF_{60} was found to be 1.69 ns, significantly longer than that of bulk N_3-COF (1.2 ns) (Figure S15), which we attribute to the fact that the nanometer-sized external diameter of N_3-COF_{60} shortens the path for electron transmission and increases the optical carrier transmission rate. Further, electrochemical impedance spectroscopy analysis revealed that N_3-COF_{60} exhibits the smallest resistance for charge transfer, again as a result of its small external diameter (Figure S16). Altogether, these data indicate excellent charge separation of electron−hole pairs in the N_3-COF_{60} nanowires under irradiation. Of note, although the N_3-COF_{80} and N_3-COF_{100} nanowires have smaller diameters than N_3-COF_{60}, they both exhibit poorer optoelectronic performance. We attribute this to the presence of larger cavities (4−6 nm) in the N_3-COF_{80} and N_3-COF_{100} nanowires, as determined from the pore size distribution analysis (Figure S7), which are indicative of defects that may inhibit the transport of carriers to the nanowire surface and increase charge transfer resistance.

We next evaluated the ability of N_3-COF_{60} to extract uranium from an aqueous solution under simulated sunlight. Samples of N_3-COF_{60} were stirred in aqueous solutions containing 10 ppm uranyl(VI) (pH values ranging from 3 to 9) and irradiated with simulated sunlight (λ = 320−780 nm, intensity of 1 kW m^{-2}). Aliquots of the solutions were collected at regular intervals, filtered, and the uranium content was analyzed using inductively coupled plasma-optical emission spectrometry (Figures S3a and S17). The maximum extraction capacity of N_3-COF_{60} was found to be 1270 mg/g from the pH = 5 solution after 7 days, more than double the capacity of N_3-COF (530 mg/g) under the same conditions and significantly more than was captured in the absence of irradiation (59 mg/g) (Figure 3a). The higher capacity of N_3-COF_{60} under simulated sunlight is a result of the light-induced external bias potential on the surface of the COF nanowires. The corresponding electric field increases the relative concentration of UO_2^{2+} ions at the surface,[10] where they can undergo reduction, and also promotes their migration and reduction in the porous architecture. A sample of N_3-COF_{60} also retained 81% of its uranium saturation capacity and exhibited no signs of structural degradation after five successive uranium extraction and elution cycles (Figure S18; see Materials and Methods for details). Of note, after 20 days of exposure to a 100 ppm uranyl(VI) solution under light irradiation, N_3-COF_{60} achieved a record saturation capacity of 10.9 g/g (Figure S19 and Table S4). In general, the capacities achieved by N_3-COF_{60} far exceed those reported for other top-performing materials designed for uranium capture from seawater (Figure 3b; Tables S3 and S5).

TEM analysis of a sample of N_3-COF_{60} following stirring in a solution of uranyl(VI) (10 ppm, pH = 5) under irradiation for 1 day revealed that uranium is evenly distributed in the nanowires (Figure S20). High-resolution TEM images revealed distinct areas with interplanar spacings of approximately 2.6 and 2.9 Å, which may correspond to different uranium compounds (Figures 4a and S20; see Results and Discussion of possible uranium uptake mechanism below). Analysis of the nanowires after 1 and 7 days of irradiation using energy-dispersive X-ray spectroscopy revealed that the amount of captured uranium increased as the exposure time increased (Figure S21). A Raman spectrum obtained for the nanowires

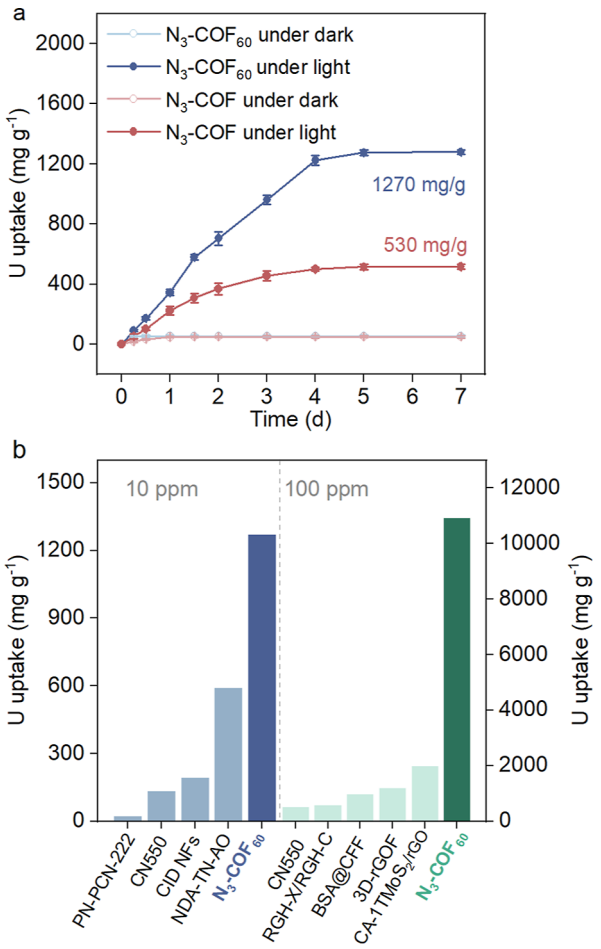

Figure 3. (a) Uranium extraction capacities of N_3-COF_{60} and N_3-COF following exposure to an aqueous solution of uranyl(VI) (10 ppm at pH = 5) under light irradiation and dark conditions; the uranium U(VI) capacity data are given in Table S2. Error bars represent the standard deviation obtained from three independent measurements. (b) A comparison of the adsorption capacity of N_3-COF_{60} exposed to 10 and 100 ppm uranyl(VI) solutions with light irradiation and the capacities of several other top-performing sorbents in the literature under similar conditions [uranyl(VI) ion concentrations of 10 and 100 ppm]. Capacities and corresponding references are summarized in Tables S3 and S5.

after 1 day of irradiation features bands at 818 and 865 cm^{-1} (Figure S22), indicative of the presence of neutral $(UO_2)O_2 \cdot 4H_2O$, and a band at 630 cm^{-1} attributed to partial oxidization of UO_2 particles; a band at 751 cm^{-1} band was assigned as γ-UO_3.[8] These features were not present in a spectrum collected for N_3-COF_{60} after exposure to a uranyl(VI) solution for 1 day in the absence of irradiation (Figure S22). A comparison of the two spectra revealed that the characteristic N−N peak for the light-irradiated sample appears at a lower energy than the corresponding peak in the dark sample, which we hypothesize is a result of the azine group serving as an electron donor for the photoreduction of uranium(VI).[21,31]

To probe the mechanism of uranium uptake in N_3-COF_{60}, we conducted a 20 day adsorption/irradiation experiment using an aqueous solution (pH = 5) containing 100 ppm of uranyl(VI) and collected nanowire samples at regular intervals for PXRD analysis. After the first day of exposure, the XRD pattern for the nanowire sample featured new diffraction peaks at 12.1, 24.9, 25.4, 27.7, 28.2, 35.0, and 35.4°, attributed to

https://doi.org/10.1021/jacs.4c07699
J. Am. Chem. Soc. 2024, 146, 23566−23573

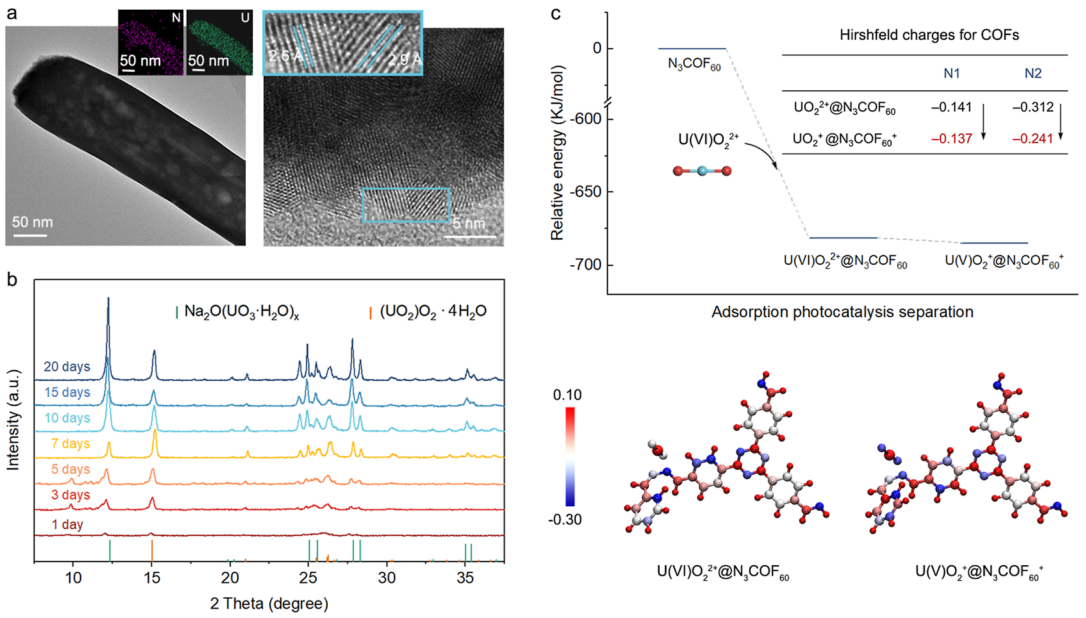

Figure 4. (a) TEM image of N_3-COF_{60} after exposure to a 10 ppm uranyl ion solution (pH = 5) under light irradiation for 7 days. High-resolution TEM image (right) showing two sizes of interplanar spacing of ∼2.6 and 2.9 Å. The mapping images show that the adsorbed uranium is evenly distributed. (b) PXRD patterns (Cu Kα radiation, λ = 1.5418 Å) obtained for samples of N_3-COF_{60} after exposure to a 100 ppm uranium(VI) solution (pH = 5) over the course of 20 days under light irradiation. Clear changes in the diffraction patterns reveal the gradual formation of $Na_2O(UO_3{\cdot}H_2O)_x$ and $(UO_2)O_2{\cdot}4H_2O$ following photoreduction of uranyl(VI) by N_3-COF_{60} and disproportionation of the resulting uranium(V) species (see Figure S24). (c) The free energy diagram of uranium adsorption and reduction on N_3-COF_{60}, and the calculated Hirshfeld charges for $U(VI)O_2^{2+}@N_3COF_{60}$ and $U(V)O_2^{+}@N_3COF_{60}^{+}$. The Hirshfeld charge distribution of $U(VI)O_2^{2+}@N_3COF_{60}$ and $U(V)O_2^{+}@N_3COF_{60}^{+}$.

$Na_2O(U^{VI}O_3{\cdot}H_2O)_x$, as well as peaks at 15.1 and 26.3° assigned to uranyl peroxide, $(U^{VI}O_2)O_2{\cdot}4H_2O$ (Figure 4b). Over the course of 20 days, the characteristic peaks associated with $Na_2O(UO_3{\cdot}H_2O)_x$ and $(UO_2)O_2{\cdot}4H_2O$ became progressively sharper, indicating the gradual generation of these two insoluble uranium compounds within the COF network.

As an additional probe of the uranium species formed under these conditions, we collected X-ray photoelectron spectra (XPS) for N_3-COF_{60} exposed to a 100 ppm uranyl(VI) solution after 30 and 240 min of irradiation. As shown in Figure S23, a satellite peak was present at ∼9 eV above the $4f_{7/2}$ emission peak in the spectrum collected after 30 min, which is diagnostic of the formation of uranium(V) species, whereas after 240 min satellite peaks were apparent at ∼4 and 10 eV above the $4f_{7/2}$ peak, indicative of uranium(VI).[32,33] Based on these results and those from PXRD analysis, we propose a plausible mechanism for uranium extraction by N_3-COF_{60} leading to the two observed products. Initially, uranyl(VI) is reduced by photoexcited N_3-COF_{60} to form uranyl(V), which then disproportionate to form $Na_2O(UO_3{\cdot}H_2O)_x$ (in the presence of sodium ions derived from NaOH)[34,35] and UO_2, which then forms $(UO_2)O_2{\cdot}4H_2O$[36] in the presence of O_2 (Figure S24).

The free energy diagrams for uranium adsorption and reduction on N_3-COF_{60} have been calculated, based on the organic fragment of N_3COF_{60}. As shown in Figures 4c and S25, UO_2^{2+} ion could be adsorbed on the N−N site of N_3COF_{60}. Subsequently, uranium(VI) was able to be spontaneously reduced to uranium(V) on N_3COF_{60}, a result that explains the excellent photocatalytic performance of N_3COF_{60} for the extraction of uranium.[37] After the photocatalytic reaction, the Hirshfeld charges at both the N1 and N2 sites of N_3COF_{60} were decreased (Figure 4c), confirming that N−N was the electron transfer site during photocatalysis.[38,39]

We next examined the performance of the N_3-COF_{60} nanowires for uranium capture from commercial seawater (pH = 8.2) containing 3.3 ppb of uranium(VI) and numerous competing ions (9500 ppm of Na^+, 1130 ppm of Mg^{2+}, 360 ppm of Ca^{2+}, 350 ppm of K^+, 499 ppb of Sr^{2+}, 28 ppb of Cu^{2+}, 5 ppb of V^{5+} [present as $H_2VO_4^-$ and HVO_4^{2-} at pH = 8.2],[40] 0.5 ppb of Ni^{2+}, 0.5 ppb Fe^{3+}, 0.1 ppb of Co^{2+}, 8000 ppm of Cl^-, and 2400 ppm of SO_4^{2-}). Under 1 kW m^{-2} simulated sunlight, N_3-COF_{60} adsorbed 22.7 mg/g uranium after 2 days, and the capacity increased to 34.5 mg/g after 42 days. Additionally, N_3-COF_{60} exhibited excellent selectivity for uranium over Fe^{3+}, Co^{2+}, Ni^{2+}, and Cu^{2+} and moderate selectivity over vanadium (Figure 5a,b and Table S6). Overall, the rate of uranium uptake in N_3-COF_{60} is significantly greater than in materials studied to date that capture uranium via physical adsorption alone or through photoreduction (Figure 5c; see Table S7 for details). Significantly, this performance in seawater also exceeds the commercial benchmark that has been established for seawater extraction of uranium to be competitive with land-based uranium mining (a one-run uptake capacity of 30 mg/g).[41]

CONCLUSIONS

In summary, we have synthesized COF nanowires of varying diameters based on the triazine-linked two-dimensional material N_3-COF[22] using a solvent modulation approach. Nanowires with diameters on the order of 100 nm exhibit excellent photoactivity and, under irradiation, efficiently capture uranium(VI) from aqueous solutions, including natural seawater, via a mechanism involving initial photoreduction to uranium(V). The uranium uptake of the nanowires significantly exceeds that achieved by other materials reported for uranium capture to date, and the uptake from seawater establishes N_3-COF_{60} as a viable candidate for commercial

https://doi.org/10.1021/jacs.4c07699
J. Am. Chem. Soc. 2024, 146, 23566−23573

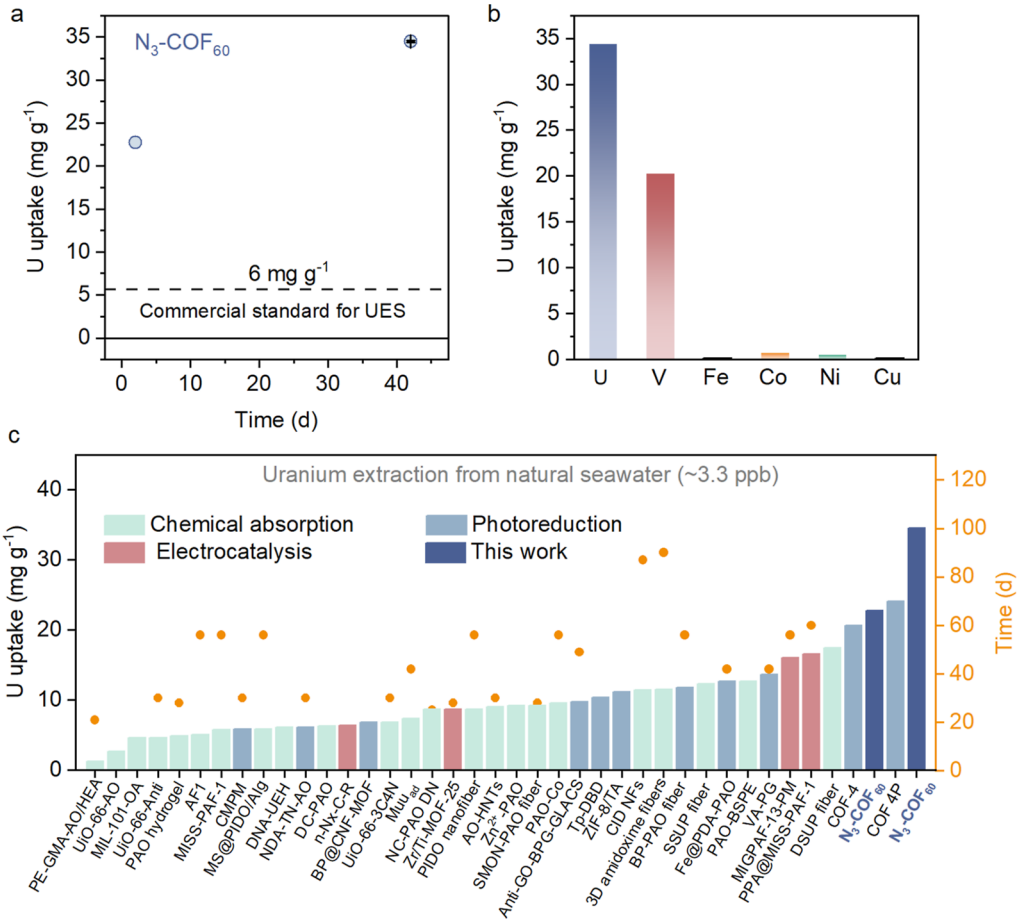

Figure 5. (a) Uranium extraction capacity of N_3-COF_{60} under light during 42 days of close contact with sterilized seawater (uranyl ion concentration of 3.3 ppb). Error bars represent the standard deviation obtained from three independent measurements. (b) Comparison of the uptake of U^{6+}, V^{5+}, Fe^{3+}, Co^{2+}, Ni^{2+}, and Cu^{2+} in N_3-COF_{60} after irradiation in commercial seawater for 42 days. (c) Uranium(VI) adsorption capacities from seawater [uranyl(VI) ion concentrations of 3.0−3.3 ppb] reported for several top-performing materials after various exposure times along with the capacities determined for N_3-COF_{60} after irradiation in seawater for 2 and 42 days (see Table S7 for details). Capacities are indicated by the height of the individual bars, and the exposure times are indicated by the purple symbols in each case.

capture applications. Our results indicate that COF nanowires may be a promising technology for extracting uranium from seawater, and future work would benefit from optimizing the synthesis of the nanowires developed here at larger scales and studying the scalability of the capture process.

EXPERIMENTAL SECTION

Synthesis of N_3-COF Nanowires. A 10 mL pressure glass tube was charged with 1,3,5-trialdehyde phenyltriazine (25 mg, 0.065 mmol), 1 − x/100 mL mesitylene and 1,4-dioxane (1:1), x/100 mL n-butanol (x = 20, 40, 60, 80 and 100) and 100 μL aqueous 6 M acetic acid. To the suspension, hydrazine hydrate (5 μL, 50−60% solution) was then added. The tube was then sealed and heated in a blast oven at 120 °C for 3 days at autogenous pressure. Thereafter, the tube was opened and the suspension was filtered and washed with chloroform (2 × 5 mL), acetone (2 × 5 mL), and tetrahydrofuran (2 × 5 mL). The solid was dried at room temperature under a vacuum to afford N_3-COF_x (x = 20, 40, 60, 80, 100) as a light-yellow powder. N_3-COF_{20} (yield: 77.1%, 19.1 mg), N_3-COF_{40} (yield: 73.7%, 18.2 mg), N_3-COF_{60} (yield: 70.5%, 17.5 mg), N_3-COF_{80} (yield: 69.2%, 17.2 mg), N_3-COF_{100} (yield: 66.5%, 16.5 mg).

ASSOCIATED CONTENT

Supporting Information

The Supporting Information is available free of charge at https://pubs.acs.org/doi/10.1021/jacs.4c07699.

Synthesis procedures, experiment details, and characterizations of materials, including SEM images, mapping images, PXRD patterns, TGA analysis, BET analysis, XPS data, Raman data, and additional calculation results (PDF)

AUTHOR INFORMATION

Corresponding Authors

Ye Yuan − *Key Laboratory of Polyoxometalate and Reticular Material Chemistry of Ministry of Education, Faculty of Chemistry, Northeast Normal University, Changchun 130024, China;* orcid.org/0000-0002-0298-2023; Email: Yuany101@nenu.edu.cn

Jeffrey R. Long − *Department of Chemistry, University of California, Berkeley, Berkeley, California 94720, United States; Department of Chemical and Biomolecular Engineering and Department of Materials Science and Engineering, University of California, Berkeley, Berkeley, California 94720, United States; Materials Sciences Division,*

Lawrence Berkeley National Laboratory, Berkeley, California 94720, United States; orcid.org/0000-0002-5324-1321; Email: jrlong@berkeley.edu

Guangshan Zhu − *Key Laboratory of Polyoxometalate and Reticular Material Chemistry of Ministry of Education, Faculty of Chemistry, Northeast Normal University, Changchun 130024, China*; Email: Zhugs@nenu.edu.cn

Authors

Xujiao Ma − *Key Laboratory of Polyoxometalate and Reticular Material Chemistry of Ministry of Education, Faculty of Chemistry, Northeast Normal University, Changchun 130024, China*

Katie R. Meihaus − *Department of Chemistry, University of California, Berkeley, Berkeley, California 94720, United States*

Yajie Yang − *Key Laboratory of Polyoxometalate and Reticular Material Chemistry of Ministry of Education, Faculty of Chemistry, Northeast Normal University, Changchun 130024, China;* orcid.org/0000-0002-9990-117X

Yue Zheng − *Key Laboratory of Polyoxometalate and Reticular Material Chemistry of Ministry of Education, Faculty of Chemistry, Northeast Normal University, Changchun 130024, China*

Fengchao Cui − *Key Laboratory of Polyoxometalate and Reticular Material Chemistry of Ministry of Education, Faculty of Chemistry, Northeast Normal University, Changchun 130024, China;* orcid.org/0009-0004-3882-0888

Jixiang Li − *Shanghai Advanced Research Institute, Chinese Academy of Sciences, Shanghai 201210, China; University of Chinese Academy of Sciences, Beijing 100049, China*

Yanqin Zhao − *Shanghai Advanced Research Institute, Chinese Academy of Sciences, Shanghai 201210, China*

Biao Jiang − *Shanghai Advanced Research Institute, Chinese Academy of Sciences, Shanghai 201210, China*

Complete contact information is available at: https://pubs.acs.org/10.1021/jacs.4c07699

Notes

The authors declare no competing financial interest.

■ ACKNOWLEDGMENTS

This research was funded by the National Key R&D Program of China (2022YFB3805902, 2022YFB3805900), the National Natural Science Foundation of China (22131004, U21A20330, 22322501, 21975039, and 52204389) and the "111" project (B18012); the Fundamental Research Funds for the Central Universities (2412020ZD008 and GFPY202309), the CNNC Key Laboratory on Uranium Extraction from Seawater (KLUES202202); the Science & Technology Department of Jilin Province (no. 20230101023JC); and the Leading Scientific Research Project from China National Nuclear Corporation (CNNC-CXLM-202205). Contributions of K.R.M. and J.R.L. were supported by the University of California, Berkeley.

■ REFERENCES

(1) Wanner, B.; Taniguchi, R. *Nuclear Power*; International Energy Agency, 2023. https://www.iea.org/energy-system/electricity/nuclear-power (accessed 12, 2023).

(2) Fraser, P.; et al. *Nuclear Power and Secure Energy Transitions: From Today's Challenges to Tomorrow's Clean Energy Systems*; International Energy Agency, 2023. https://www.iea.org/reports/nuclear-power-and-secure-energy-transitions (accessed 12, 2023).

(3) Sholl, D. S.; Lively, R. P. Seven Chemical Separations to Change the World. *Nature* **2016**, *532* (7600), 435−437.

(4) Chu, S.; Majumdar, A. Opportunities and Challenges for a Sustainable Energy Future. *Nature* **2012**, *488* (7411), 294−303.

(5) Hoffert, M. I.; Caldeira, K.; Benford, G.; Criswell, D. R.; Green, C.; Herzog, H.; Jain, A. K.; Kheshgi, H. S.; Lackner, K. S.; Lewis, J. S.; Lightfoot, H. D.; Manheimer, W.; Mankins, J. C.; Mauel, M. E.; Perkins, L. J.; Schlesinger, M. E.; Volk, T.; Wigley, T. M. L. Advanced Technology Paths to Global Climate Stability: Energy for a Greenhouse Planet. *Science* **2002**, *298* (5595), 981−987.

(6) Sun, Q.; Aguila, B.; Perman, J.; Ivanov, A. S.; Bryantsev, V. S.; Earl, L. D.; Abney, C. W.; Wojtas, L.; Ma, S. Bio-Inspired Nano-Traps for Uranium Extraction from Seawater and Recovery from Nuclear Waste. *Nat. Commun.* **2018**, *9* (1), 1644.

(7) Cui, W.-R.; Li, F.-F.; Xu, R.-H.; Zhang, C.-R.; Chen, X.-R.; Yan, R.-H.; Liang, R.-P.; Qiu, J.-D. Regenerable Covalent Organic Frameworks for Photo-Enhanced Uranium Adsorption from Seawater. *Angew. Chem., Int. Ed.* **2020**, *59* (40), 17684−17690.

(8) Liu, C.; Hsu, P.-C.; Xie, J.; Zhao, J.; Wu, T.; Wang, H.; Liu, W.; Zhang, J.; Chu, S.; Cui, Y. A Half-Wave Rectified Alternating Current Electrochemical Method for Uranium Extraction from Seawater. *Nat. Energy* **2017**, *2* (4), 17007.

(9) *Energy, Electricity and Nuclear Power Estimates for the Period up to 2050, Reference Data Series No. 1, IAEA, Vienna*; International Atomic Energy Agency, 2016. https://www.iaea.org/publications/11120/energy-electricity-and-nuclear-power-estimates-for-the-period-up-to-2050 (accessed 12, 2023).

(10) Davies, R. V.; Kennedy, J.; McIlroy, R. W.; Spence, R.; Hill, K. M. Extraction of Uranium from Sea Water. *Nature* **1964**, *203* (4950), 1110−1115.

(11) Abney, C. W.; Mayes, R. T.; Saito, T.; Dai, S. Materials for the Recovery of Uranium from Seawater. *Chem. Rev.* **2017**, *117* (23), 13935−14013.

(12) Cui, W.-R.; Zhang, C.-R.; Jiang, W.; Li, F.-F.; Liang, R.-P.; Liu, J.; Qiu, J.-D. Regenerable and Stable Sp2 Carbon-Conjugated Covalent Organic Frameworks for Selective Detection and Extraction of Uranium. *Nat. Commun.* **2020**, *11* (1), 436.

(13) Yuan, Y.; Yang, Y.; Ma, X.; Meng, Q.; Wang, L.; Zhao, S.; Zhu, G. Molecularly Imprinted Porous Aromatic Frameworks and Their Composite Components for Selective Extraction of Uranium Ions. *Adv. Mater.* **2018**, *30* (12), 1706507.

(14) Ivanov, A. S.; Leggett, C. J.; Parker, B. F.; Zhang, Z.; Arnold, J.; Dai, S.; Abney, C. W.; Bryantsev, V. S.; Rao, L. Origin of the Unusually Strong and Selective Binding of Vanadium by Polyamidoximes in Seawater. *Nat. Commun.* **2017**, *8* (1), 1560.

(15) Yuan, Y.; Niu, B.; Yu, Q.; Guo, X.; Guo, Z.; Wen, J.; Liu, T.; Zhang, H.; Wang, N. Photoinduced Multiple Effects to Enhance Uranium Extraction from Natural Seawater by Black Phosphorus Nanosheets. *Angew. Chem., Int. Ed.* **2020**, *59* (3), 1220−1227.

(16) Zhang, H.; Liu, W.; Li, A.; Zhang, D.; Li, X.; Zhai, F.; Chen, L.; Chen, L.; Wang, Y.; Wang, S. Three Mechanisms in One Material: Uranium Capture by a Polyoxometalate−Organic Framework through Combined Complexation, Chemical Reduction, and Photocatalytic Reduction. *Angew. Chem., Int. Ed.* **2019**, *58* (45), 16110−16114.

(17) Cui, W.-R.; Zhang, C.-R.; Xu, R.-H.; Chen, X.-R.; Yan, R.-H.; Jiang, W.; Liang, R.-P.; Qiu, J.-D. Low Band Gap Benzoxazole-Linked Covalent Organic Frameworks for Photo-Enhanced Targeted Uranium Recovery. *Small* **2021**, *17* (6), 2006882.

(18) Zhang, T.; Xing, G.; Chen, W.; Chen, L. Porous Organic Polymers: A Promising Platform for Efficient Photocatalysis. *Mater. Chem. Front.* **2020**, *4* (2), 332−353.

(19) Wan, Y.; Wang, L.; Xu, H.; Wu, X.; Yang, J. A. A Simple Molecular Design Strategy for Two-Dimensional Covalent Organic Framework Capable of Visible-Light-Driven Water Splitting. *J. Am. Chem. Soc.* **2020**, *142* (9), 4508−4516.

(20) Wang, H.; Wang, H.; Wang, Z.; Tang, L.; Zeng, G.; Xu, P.; Chen, M.; Xiong, T.; Zhou, C.; Li, X.; Huang, D.; Zhu, Y.; Wang, Z.; Tang, J. Covalent Organic Framework Photocatalysts: Structures and Applications. *Chem. Soc. Rev.* **2020**, *49* (12), 4135−4165.
(21) Nikoobakht, B.; Wang, X.; Herzing, A.; Shi, J. Scalable Synthesis and Device Integration of Self-Registered One-Dimensional Zinc Oxide Nanostructures and Related Materials. *Chem. Soc. Rev.* **2013**, *42* (1), 342−365.
(22) Vyas, V. S.; Haase, F.; Stegbauer, L.; Savasci, G.; Podjaski, F.; Ochsenfeld, C.; Lotsch, B. V. A Tunable Azine Covalent Organic Framework Platform for Visible Light-Induced Hydrogen Generation. *Nat. Commun.* **2015**, *6* (1), 8508.
(23) Cao, L.; Wu, H.; Cao, Y.; Fan, C.; Zhao, R.; He, X.; Yang, P.; Shi, B.; You, X.; Jiang, Z. Weakly Humidity-Dependent Proton-Conducting Cof Membranes. *Adv. Mater.* **2020**, *32* (52), 2005565.
(24) Wang, S.; Zhang, Z.; Zhang, H.; Rajan, A. G.; Xu, N.; Yang, Y.; Zeng, Y.; Liu, P.; Zhang, X.; Mao, Q.; He, Y.; Zhao, J.; Li, B.-G.; Strano, M. S.; Wang, W.-J. Reversible Polycondensation-Termination Growth of Covalent-Organic-Framework Spheres, Fibers, and Films. *Matter* **2019**, *1* (6), 1592−1605.
(25) Wang, S.; Xu, X.; Yue, Y.; Yu, K.; Shui, Q.; Huang, N.; Chen, H. Semiconductive Covalent Organic Frameworks: Structural Design, Synthesis, and Application. *Small Struct.* **2020**, *1* (2), 2000021.
(26) Evans, A. M.; Parent, L. R.; Flanders, N. C.; Bisbey, R. P.; Vitaku, E.; Kirschner, M. S.; Schaller, R. D.; Chen, L. X.; Gianneschi, N. C.; Dichtel, W. R. Seeded Growth of Single-Crystal Two-Dimensional Covalent Organic Frameworks. *Science* **2018**, *361* (6397), 52−57.
(27) Liu, M.; Wang, Y.-R.; Ding, H.-M.; Lu, M.; Gao, G.-K.; Dong, L.-Z.; Li, Q.; Chen, Y.; Li, S.-L.; Lan, Y.-Q. Self-Assembly of Anthraquinone Covalent Organic Frameworks as 1d Superstructures for Highly Efficient Co2 Electroreduction to Ch4. *Sci. Bull.* **2021**, *66* (16), 1659−1668.
(28) Alivisatos, A. P. Semiconductor Clusters, Nanocrystals, and Quantum Dots. *Science* **1996**, *271* (5251), 933−937.
(29) Kahn, A. Fermi Level, Work Function and Vacuum Level. *Mater. Horiz.* **2016**, *3* (1), 7−10.
(30) Lakowicz, J. R.; Ray, K.; Chowdhury, M.; Szmacinski, H.; Fu, Y.; Zhang, J.; Nowaczyk, K. Plasmon-Controlled Fluorescence: A New Paradigm in Fluorescence Spectroscopy. *Analyst* **2008**, *133* (10), 1308−1346.
(31) Zheng, Y.; Jiao, Y.; Zhu, Y.; Li, L. H.; Han, Y.; Chen, Y.; Du, A.; Jaroniec, M.; Qiao, S. Z. Hydrogen Evolution by a Metal-Free Electrocatalyst. *Nat. Commun.* **2014**, *5* (1), 3783.
(32) Gouder, T.; Eloirdi, R.; Caciuffo, R. Direct Observation of Pure Pentavalent Uranium in U_2O_5 Thin Films by High Resolution Photoemission Spectroscopy. *Sci. Rep.* **2018**, *8* (1), 8306.
(33) Ilton, E. S.; Bagus, P. S. XPS Determination of Uranium Oxidation States. *Surf. Interface Anal.* **2011**, *43* (13), 1549−1560.
(34) Yang, H.; Liu, X.; Hao, M.; Xie, Y.; Wang, X.; Tian, H.; Waterhouse, G. I. N.; Kruger, P. E.; Telfer, S. G.; Ma, S. Functionalized Iron−Nitrogen−Carbon Electrocatalyst Provides a Reversible Electron Transfer Platform for Efficient Uranium Extraction from Seawater. *Adv. Mater.* **2021**, *33* (51), 2106621.
(35) Liu, X.; Xie, Y.; Hao, M.; Chen, Z.; Yang, H.; Waterhouse, G. I. N.; Ma, S.; Wang, X. Highly Efficient Electrocatalytic Uranium Extraction from Seawater over an Amidoxime-Functionalized in−N−C Catalyst. *Adv. Sci.* **2022**, *9* (23), 2201735.
(36) Corbel, C.; Sattonnay, G.; Guilbert, S.; Garrido, F.; Barthe, M. F.; Jegou, C. Addition Versus Radiolytic Production Effects of Hydrogen Peroxide on Aqueous Corrosion of UO_2. *J. Nucl. Mater.* **2006**, *348* (1−2), 1−17.
(37) Chen, Z.; Wang, J.; Hao, M.; Xie, Y.; Liu, X.; Yang, H.; Waterhouse, G. I. N.; Wang, X.; Ma, S. Tuning Excited State Electronic Structure and Charge Transport in Covalent Organic Frameworks for Enhanced Photocatalytic Performance. *Nat. Commun.* **2023**, *14* (1), 1106.
(38) Lu, T.; Chen, F. Atomic Dipole Moment Corrected Hirshfeld Population Method. *J. Theor. Comput. Chem.* **2012**, *11* (01), 163−183.
(39) Lu, T.; Chen, F. Multiwfn: A Multifunctional Wavefunction Analyzer. *J. Comput. Chem.* **2012**, *33* (5), 580−592.
(40) Simon, F. X.; Berdalet, E.; Gracia, F. A.; España, F.; Llorens, J. Seawater Disinfection by Chlorine Dioxide and Sodium Hypochlorite. A Comparison of Biofilm Formation. *Water, Air, Soil Pollut.* **2014**, *225* (4), 1921.
(41) Kim, J.; Tsouris, C.; Oyola, Y.; Janke, C. J.; Mayes, R. T.; Dai, S.; Gill, G.; Kuo, L.-J.; Wood, J.; Choe, K.-Y.; Schneider, E.; Lindner, H. Uptake of Uranium from Seawater by Amidoxime-Based Polymeric Adsorbent: Field Experiments, Modeling, and Updated Economic Assessment. *Ind. Eng. Chem. Res.* **2014**, *53* (14), 6076−6083.

https://doi.org/10.1021/jacs.4c07699
J. Am. Chem. Soc. 2024, 146, 23566−23573